A Flatness-Based Trajectory Planning Algorithm for Rendezvous of Single-Thruster Spacecraft ⋆

Julio C. Sanchez* **Francisco Gavilan*** **Rafael Vazquez*** **Christophe Louembet****

* *Departamento de Ingeniería Aeroespacial, Universidad de Sevilla, Seville, Spain (e-mails: jsanchezm@us.es, fgavilan@us.es, rvazquez1@us.es).*
** *LAAS-CNRS, Université de Toulouse, CNRS, Toulouse, France (e-mail: louembet@laas.fr)*

Abstract: This work presents a trajectory planning algorithm for spacecraft rendezvous with a passive target. The main assumption is that the chaser vehicle has a single thruster and an attitude control system (e.g. reaction wheels) providing the necessary torque to change its orientation, which may be the situation for small spacecraft or in the case of thruster failure. The goal is to design fuel-optimal manoeuvres while satisfying operational constraints. This time-continuous optimal control problem is addressed using the translational state transition matrix and the attitude flatness property to transform the dynamics into algebraic relations. Then, the problem is transformed to a non-linear programming problem which has to be solved. Simulation results are showed and discussed.

Keywords: Spacecraft autonomy, Space robotics, Trajectory planning, Optimal trajectory, Constrained control.

1. INTRODUCTION

Autonomous spacecraft rendezvous and docking is becoming a more important concern in the space industry as access to space continues increasing, see Woffinden and Geller (2007) for an historical review or Fehse (2003) for the basics. Nowadays, an increasing interest to demonstrate autonomous rendezvous and flight formation operations for lightweight and low-power spacecraft is arising with CPOD, PRISMA and PROBA-3 missions as examples, see Bowen et al. (2015); Persson et al. (2006); Castellani et al. (2013).

Typically, the rendezvous problem has been widely studied just considering orbit control making the assumption that translational and rotational motion are decoupled. Direct transcription methods which transform the optimal control problem into a discrete optimization problem have been used in many works as Gavilan et al. (2012); Vazquez et al. (2017) among others. However, orbit and attitude control subsystems are mutually coupled, which is mainly due to the dependence of the thrusters orientation with the relative attitude between target and pursuer (at least in the short-term). Strategies based on feedback considering a single-thruster and three reaction wheels as in Oland et al. (2013) and a six thrusters cuboid layout as in Zhang and Duan (2012) have been the most employed approaches. Concerning optimal control, Moon et al. (2016) obtained a suboptimal solution for a single-thruster configuration solving the translational problem with an indirect method and using a quaternion-feedback controller to obtain the commanded thruster orientations.

Since the problem is governed by the thrusters orientation, an overview of the existing attitude planning methods for spin-to-spin manoeuvres is required. Model Predictive Control (MPC) techniques based on linearization around a set point have been used in the works of Øyvind Hegrenæs et al. (2005); Guiggiani et al. (2015). An interesting approach is the one followed by Louembet et al. (2009); Caubet and Biggs (2015) based on the attitude dynamics flatness property (see Fliess et al. (1995) for more details about flatness theory). This property allowed them to parameterize the state and then directly obtain a closed form expression of the torque via inverse dynamics to pose a non-linear programming (NLP) problem.

In this paper, a single-thruster spacecraft equipped with an attitude control system (ACS) is considered. The proposed methodology consists in solving the optimal control problem as an equivalent static program using the formal state transition for the relative translation motion and the flatness property of the attitude motion.

The structure of this paper is as follows. Section 2 describes the coupled translational and rotational model for spacecraft rendezvous. Next, Section 3 presents the time-continuous rendezvous problem with its constraints and objective function. Section 4 describes the techniques employed to solve the optimal control problem. Section 5

⋆ The authors gratefully acknowledge Universidad de Sevilla for funding part of this work through under its V-PPI US. Rafael Vazquez acknowledges financial support of the Spanish Ministerio de Economía y Competitividad under grant MTM2015-65608-P.

shows results for cases of interest. Finally, Section 6 closes this paper with some additional considerations.

2. 6-DOF MODEL OF SPACECRAFT RENDEZVOUS

In this section, a six-degrees of freedom model for spacecraft rendezvous is presented. Firstly, the translational relative motion between the vehicles is derived; secondly, the model for the rotational motion of the chaser is described; and finally, the coupling between both motions is obtained.

2.1 Translational motion

The linear Hill-Clohessy-Wiltshire (HCW) equations (see Clohessy and Wiltshire (1960)) assume that the target vehicle is moving along a circular orbit of radius R. Thus the angular speed of the target is $n{=}\sqrt{\mu/R^3}$ where μ is the gravitation parameter of the Earth, $\mu{=}398600.4$ km^3/s^2. Considering a local-vertical/local-horizontal (LVLH) frame of reference fixed on the center of gravity of the target vehicle where x refers to the in-track position, y to the cross-track position and z to the radial position (positive pointing towards the centre of the Earth), the HCW equations are

$$\ddot{x} = 2n\dot{z}, \tag{1}$$

$$\ddot{y} = -n^2 y, \tag{2}$$

$$\ddot{z} = 3n^2 z - 2n\dot{x}. \tag{3}$$

Modelling propulsion as impulses

$$\mathbf{u}(t) = \sum_{k=1}^{N_p} \mathbf{u}_k \delta(t - t_k), \tag{4}$$

and solving (1)-(3) leads to an exact propagation by means of the state transition matrix

$$\mathbf{x}(t) = \mathbf{A}(t, t_0)\mathbf{x}(t_0) + \mathbf{B}\mathbf{u}(t), \tag{5}$$

being $\mathbf{x}(t){=}[x(t), y(t), z(t), \dot{x}(t), \dot{y}(t), \dot{z}(t)]^T$ and $\mathbf{u}(t) = [u_x(t), u_y(t), u_z(t)]^T$. The $\mathbf{A}$ and $\mathbf{B}$ matrices are given by

$$\mathbf{A} = \begin{bmatrix} 1 & 0 & 6(nT-S) & \frac{4S}{n} - 3T & 0 & \frac{2(1-C)}{n} \\ 0 & C & 0 & 0 & \frac{S}{n} & 0 \\ 0 & 0 & 4-3C & \frac{2(C-1)}{n} & 0 & \frac{S}{n} \\ 0 & 0 & 6n(1-C) & 4C-3 & 0 & 2S \\ 0 & -nS & 0 & 0 & C & 0 \\ 0 & 0 & 3nS & -2S & 0 & C \end{bmatrix}, \tag{6}$$

and $\mathbf{B}{=}[\mathbf{\Theta}_{3\times3}, \mathbf{Id}_{3\times3}]^T$.We have denoted $T{=}t\text{-}t_0$, $S{=}\sin nT$, $C{=}\cos nT$, $\mathbf{\Theta}$ and $\mathbf{Id}$ as a full of zeros and identity matrix respectively.

2.2 Rotational motion

The modified Rodrigues parameters (MRP) representation (see Marandi and Modi (1987) for more details about MRP), is chosen. MRP have the advantage of being a minimal attitude representation which avoids the unit-norm quaternion constraint. The MRP are denoted as $\boldsymbol{\sigma}{=}[\sigma_1, \sigma_2, \sigma_3]^T$, and its relation with the rotation angle, θ_{rot}, and axis $\mathbf{e}$, is $\boldsymbol{\sigma}{=}\mathbf{e}\tan(\theta_{rot}/4)$. Singularities arise when $\theta_{rot}{=}\pm2\pi$ but they can be avoided by constraining $\theta_{rot}{\in}(-2\pi,\ 2\pi)$.

MRP composition rule between attitudes is as follows

$$\begin{aligned} &\boldsymbol{\sigma}_{S''/S} = \\ &\left[(1 - \|\boldsymbol{\sigma}_{S''/S'}\|_2^2)\boldsymbol{\sigma}_{S'/S} + (1 - \|\boldsymbol{\sigma}_{S'/S}\|_2^2)\boldsymbol{\sigma}_{S''/S'}\right. \\ &+2\boldsymbol{\sigma}_{S'/S} \times \boldsymbol{\sigma}_{S''/S'}\big] \big[1 + (\|\boldsymbol{\sigma}_{S'/S}\|_2 \|\boldsymbol{\sigma}_{S''/S'}\|_2)^2 \\ &\left.-2\boldsymbol{\sigma}_{S'/S} \cdot \boldsymbol{\sigma}_{S''/S'}\right]^{-1}, \end{aligned} \tag{7}$$

where attitudes between S'/S and S''/S' frames of reference are employed to obtain the attitude between S''/S.

Rotational motion kinematic and dynamic equations expressed in a frame of reference fixed on the center of gravity of the chaser vehicle are

$$\dot{\boldsymbol{\sigma}} = \mathbf{C}(\boldsymbol{\sigma})\boldsymbol{\omega}, \tag{8}$$

$$\mathbf{I}\,\dot{\boldsymbol{\omega}} + \boldsymbol{\omega} \times \mathbf{I}\boldsymbol{\omega} = \mathbf{M}, \tag{9}$$

where $\boldsymbol{\omega}$ is the angular velocity vector, $\mathbf{M}$ the torque vector, $\mathbf{I}$ the chaser spacecraft inertia matrix and $\mathbf{C}(\boldsymbol{\sigma})$ has the following expression

$$\mathbf{C} = \begin{bmatrix} 1+\sigma_1^2-\sigma_2^2-\sigma_3^2 & 2(\sigma_1\sigma_2-\sigma_3) & 2(\sigma_1\sigma_3+\sigma_2) \\ 2(\sigma_1\sigma_2+\sigma_3) & 1-\sigma_1^2+\sigma_2^2-\sigma_3^2 & 2(\sigma_2\sigma_3-\sigma_1) \\ 2(\sigma_1\sigma_3-\sigma_2) & 2(\sigma_2\sigma_3+\sigma_1) & 1-\sigma_1^2-\sigma_2^2+\sigma_3^2 \end{bmatrix}.$$

Although an ACS consisting of reaction wheels is being considered, as a simplification the external applied torque, $\mathbf{M}$, will be directly taken as control input, as in Caubet and Biggs (2015), instead of the reaction wheels angular accelerations.

2.3 Coupling between translational and rotational motion

Considering one thruster fixed on the chaser body frame, the translational and rotational motion coupling arises trough the propulsion term

$$\mathbf{u}(t) = \mathbf{R}(\boldsymbol{\sigma}(t))\mathbf{v}u(t), \tag{10}$$

where $\mathbf{v}$ is a unit vector representing the thruster orientation in the chaser body frame, u is the amplitude of the single-thruster impulse and $\mathbf{R}(\boldsymbol{\sigma})$ is the rotation matrix (between the chaser body frame and the LVLH frame) expressed by means of the MRP

$$\mathbf{R}(\boldsymbol{\sigma}) = \mathbf{Id} + \frac{8\boldsymbol{\sigma}^\times\boldsymbol{\sigma}^\times - 4(1 - \|\boldsymbol{\sigma}\|_2^2)\boldsymbol{\sigma}^\times}{\left(1 + \|\boldsymbol{\sigma}\|_2^2\right)^2}, \tag{11}$$

where $\boldsymbol{\sigma}^\times$ is the cross product matrix. Introducing (10) into (5) leads to

$$\mathbf{x}(t) = \mathbf{A}(t, t_0)\mathbf{x}(t_0) + \mathbf{B}\mathbf{R}(\boldsymbol{\sigma}(t))\mathbf{v}u(t). \tag{12}$$

Note that the propulsive action projected on the LVLH frame, $\mathbf{u}$, depends on the vehicle attitude in a non-linear way, see (10). Moreover, the relation between MRP and torque given by (8) and (9), is also non-linear.

3. RENDEZVOUS PLANNING PROBLEM

In this section, the constraints and objective function to minimize are introduced.

3.1 Constraints of the problem

LOS constraint

The LOS area is a region whose purpose is to guarantee that the chaser spacecraft is all time visible from the docking point. The LOS region can be defined by the equations $x \geq c_z(z-z_0)$, $x \geq -c_z(z+z_0)$, $x \geq c_y(y-y_0)$, $x \geq -c_y(y+y_0)$ and $x \geq 0$; these equations limit the relative position state space by five planes

$$\mathbf{A}_L \mathbf{x}(t) \leq \mathbf{b}_L, \tag{13}$$

where $\mathbf{A}_L \in \mathbb{R}^{5\times 6}$ and $\mathbf{b}_L \in \mathbb{R}^5$ summarize the LOS planes equations algebraically.

Actuators constraints

Velocity increment and torque, produced by thrusters and reaction wheels respectively, are considered to be bounded

$$0 \leq u(t) \leq u_{max}, \tag{14}$$

$$-M_{max} \leq M_i(t) \leq M_{max}, \quad i = 1,2,3. \tag{15}$$

It is assumed that thruster valves opening times can be adjusted to produce the exact impulse amplitude.

Terminal constraints

At final time, rendezvous must be accomplished which implies

$$\mathbf{x}(t_f) = \mathbf{0}. \tag{16}$$

Moreover, to ease docking operations, constraints on the final attitude and angular velocity are imposed

$$\boldsymbol{\sigma}(t_f) = \boldsymbol{\sigma}_f, \quad \boldsymbol{\omega}(t_f) = \mathbf{0}. \tag{17}$$

3.2 Objective function

The chosen objective function, J, seeks to minimize fuel consumption, which is equivalent to minimize the L^1-norm of the applied impulses

$$J = \int_{t_0}^{t_f} \|u(t)\|_1 \, dt. \tag{18}$$

3.3 Optimal control problem

Summarizing the translational dynamics (12), the rotational dynamics (8)-(9), the constraints (13)-(17) and the objective function (18), the optimization problem states as

$$\begin{aligned}
\underset{u(t),\mathbf{M}(t)}{\text{minimize}} \quad & \int_{t_0}^{t_f} \|u(t)\|_1 \, dt \\
\text{subject to} \quad & \mathbf{x}(t) = \mathbf{A}(t,t_0)\mathbf{x}_0 + \mathbf{B}\mathbf{R}(\boldsymbol{\sigma}(t))\mathbf{v}u(t), \\
& \dot{\boldsymbol{\sigma}}(t) = \mathbf{C}(\boldsymbol{\sigma}(t))\boldsymbol{\omega}(t), \\
& \mathbf{I}\dot{\boldsymbol{\omega}}(t) = \mathbf{M}(t) - \boldsymbol{\omega}(t) \times \mathbf{I}\boldsymbol{\omega}(t), \\
& \mathbf{A}_L \mathbf{x}(t) \leq \mathbf{b}_L, \\
& 0 \leq u(t) \leq u_{max}, \\
& -M_{max} \leq M_i(t) \leq M_{max}, \ \ i = 1,2,3, \\
& \mathbf{x}(t_f) = \mathbf{0}, \\
& \boldsymbol{\sigma}(t_f) = \boldsymbol{\sigma}_f, \\
& \boldsymbol{\omega}(t_f) = \mathbf{0}.
\end{aligned} \tag{19}$$

4. SINGLE-THRUSTER RENDEZVOUS OPTIMAL CONTROL COMPUTATION

In this section, the method to solve the optimal control problem (19) is presented.

4.1 Attitude flatness property

As attitude dynamics given by (8) and (9) are non-linear, accounting them in the resolution of the optimal control problem usually require numerical integration. However, this system of differential equations has the flatness property, see Louembet et al. (2009). Parameterizing the attitude representation, $\boldsymbol{\sigma}$, with respect to time, these differential equations can be transformed into algebraic relations. Inverting (8) and deriving the obtained angular velocity with respect to time

$$\boldsymbol{\omega}(t) = \mathbf{C}^{-1}(\boldsymbol{\sigma})\dot{\boldsymbol{\sigma}}, \tag{20}$$

$$\dot{\boldsymbol{\omega}}(t) = \mathbf{C}^{-1}(\boldsymbol{\sigma})\ddot{\boldsymbol{\sigma}} + \dot{\mathbf{C}}^{-1}(\dot{\boldsymbol{\sigma}},\boldsymbol{\sigma})\dot{\boldsymbol{\sigma}}, \tag{21}$$

the torque is explicitly obtained as

$$\begin{aligned}
\mathbf{M}(t) = \mathbf{I}[&\dot{\mathbf{C}}^{-1}(\dot{\boldsymbol{\sigma}},\boldsymbol{\sigma})\dot{\boldsymbol{\sigma}} + \mathbf{C}^{-1}(\boldsymbol{\sigma})\ddot{\boldsymbol{\sigma}}] \\
&+[\mathbf{C}^{-1}(\boldsymbol{\sigma})\dot{\boldsymbol{\sigma}}] \times \mathbf{I}\mathbf{C}^{-1}(\boldsymbol{\sigma})\dot{\boldsymbol{\sigma}}.
\end{aligned} \tag{22}$$

Note that time dependencies have been omitted at the right-hand side of (20)-(22) for clarity. The torque is now directly parameterized as a function of the MRP time evolution, $\mathbf{M}(t)=\mathbf{M}(\boldsymbol{\sigma}(t))$.

4.2 NLP description

Parameterizing the optimal control problem

The use of the translational state transition matrix, see (12), and the attitude flatness property, see (20)-(22), avoid numerical integration since the dynamics are replaced with algebraic equations. Dividing the manoeuvre time, $t \in [t_0, t_f]$, into N_p intervals of duration $T=(t_f - t_0)/N_p$, the following attitude parameterization based on splines (they avoid the Runge phenomenon associated with high order polynomials, see Gautschi (2012)) for each interval is chosen

$$\begin{aligned}
&\sigma_i(t) = \sum_{j=0}^{m} a_{i,j,k}(t - t_{k-1})^j, \quad i = 1,2,3, \\
&t \in [t_{k-1}, t_k], \quad t_k = t_0 + kT, \quad k = 1 \ldots N_p.
\end{aligned} \tag{23}$$

Introducing (23) into (22), the torque is parameterized in terms of the splines coefficients, $a_{i,j,k}$, for each segment k. However, splines lack of continuity at a certain degree on the nodes. Since the attitude profile must have physical meaning, C^2 continuity has to be assured. The following linear equality constraints between adjacent intervals must be added to the optimization problem

$$\boldsymbol{\sigma}(t_k, \mathbf{a}_k) = \boldsymbol{\sigma}(t_k, \mathbf{a}_{k-1}), \quad k = 2 \ldots N_p, \tag{24}$$

$$\dot{\boldsymbol{\sigma}}(t_k, \mathbf{a}_k) = \dot{\boldsymbol{\sigma}}(t_k, \mathbf{a}_{k-1}), \quad k = 2 \ldots N_p, \tag{25}$$

$$\ddot{\boldsymbol{\sigma}}(t_k, \mathbf{a}_k) = \ddot{\boldsymbol{\sigma}}(t_k, \mathbf{a}_{k-1}), \quad k = 2 \ldots N_p, \tag{26}$$

where the variable $\mathbf{a}_k \in \mathbb{R}^{3(m+1)}$ collects all the attitude coefficients for each segment

$$\begin{aligned}
\mathbf{a}_k = [&a_{1,0,k}, \ldots, a_{1,m,k}, a_{2,0,k}, \ldots, a_{2,m,k}, \\
&a_{3,0,k}, \ldots, a_{3,m,k}]^T.
\end{aligned} \tag{27}$$

Evaluating (23) at the end of each interval, the translational states propagation (12) is posed in discrete form as

$$\mathbf{x}_k = \mathbf{A}\mathbf{x}_{k-1} + \mathbf{B}\mathbf{R}(\boldsymbol{\sigma}_k)\mathbf{v}u_k, \quad k = 1 \ldots N_p, \tag{28}$$

where $\mathbf{x}_k=\mathbf{x}(t_k)$ and $\boldsymbol{\sigma}_k=\boldsymbol{\sigma}(t_k, \mathbf{a}_k)$ are the translational states and MRP values at the end of each interval, which will be denoted as nodes.

Minimal rotation path

It is desirable that the minimal rotation path, between the attitude of consecutive nodes, is chosen by the solver. This condition is enforced by constraining $\theta_{rot}\in[-\pi,\ \pi]$ which is equivalent to constrain the norm of the rotation MRP

$$\|\boldsymbol{\sigma}_{rot,k}(\boldsymbol{\sigma}_k,\boldsymbol{\sigma}_{k-1})\|_2 \leq 1. \tag{29}$$

The rotation MRP, $\boldsymbol{\sigma}_{rot,k}$, is obtained with the attitude composition rule (7) as a function of $\boldsymbol{\sigma}_k$ and $\boldsymbol{\sigma}_{k-1}$. This condition adds N_p non-linear inequality constraints.

Reduction of torque constraint

Torque constraint is considered in discrete form gridding each sampling interval k with n_M equally spaced subintervals with duration $T_M{=}T/n_M$, at which the torque constraint is imposed

$$\begin{array}{ll} -M_{max} \leq M_i(t_{k,l},\mathbf{a}_k) \leq M_{max}, & i=1,2,3, \\ t_{k,l}=t_0+(k-1)T+lT_M, & l=0\ldots n_M. \end{array} \tag{30}$$

Compact formulation

To ease the notation, following Gavilan et al. (2012), a compact formulation of the discrete problem will be developed. Defining $\mathbf{x_S}$, $\mathbf{u_S}$ and $\mathbf{a_S}$, as stack vectors containing $6N_p$ translational states, N_p impulses and $3(m+1)N_p$ attitude coefficients,

$$\mathbf{x_S}=\begin{bmatrix}\mathbf{x}_1\\ \mathbf{x}_2\\ \vdots\\ \mathbf{x}_{N_p}\end{bmatrix},\ \mathbf{u_S}=\begin{bmatrix}u_1\\ u_2\\ \vdots\\ u_{N_p}\end{bmatrix},\ \mathbf{a_S}=\begin{bmatrix}\mathbf{a}_1\\ \mathbf{a}_2\\ \vdots\\ \mathbf{a}_{N_p}\end{bmatrix}, \tag{31}$$

the matrices

$$\mathbf{F}=\left[\ \mathbf{A},\ \mathbf{A}^2,\ \ldots,\ \mathbf{A}^{N_p}\ \right]^T, \tag{32}$$

and $\mathbf{G}$ as a block lower triangular matrix with its non-null elements defined by $\mathbf{G}_{ik}{=}\mathbf{A}^{i-k}\mathbf{B}\mathbf{R}_{\mathbf{a}_k}\mathbf{v}$. The matrix $\mathbf{R}_{\mathbf{a}_k}{=}\mathbf{R}(\boldsymbol{\sigma}(t_k,\mathbf{a}_k))$ is the MRP rotation matrix evaluated at the node k. The relation between the stack vectors and matrices defined in (31)-(32) is given by

$$\mathbf{x_S}=\mathbf{F}\mathbf{x}_0+\mathbf{G}(\mathbf{a_S})\mathbf{u_S}. \tag{33}$$

Discrete optimization problem

The time-continuous optimization problem (19) is now posed in discrete form as

$$\begin{array}{ll} \underset{\mathbf{u_S},\,\mathbf{a_S}}{\text{minimize}} & \|\mathbf{u_S}\|_1 \\ \text{subject to} & \mathbf{A}_{LS}\mathbf{G}(\mathbf{a_S})\mathbf{u_S}\leq\mathbf{b}_{LS}-\mathbf{F}\mathbf{x}_0, \\ & \mathbf{0}\leq\mathbf{u_S}\leq\mathbf{u_S}_{max}, \\ & -M_{max}\leq M_i(t_{k,l},\mathbf{a}_k)\leq M_{max}, \\ & \mathbf{A}_{rend}\mathbf{G}(\mathbf{a_S})\mathbf{u_S}=-\mathbf{A}_{rend}\mathbf{F}\mathbf{x}_0, \\ & \boldsymbol{\sigma}(t_0,\mathbf{a}_1)=\boldsymbol{\sigma}_0, \\ & \dot{\boldsymbol{\sigma}}(t_0,\mathbf{a}_1)=\dot{\boldsymbol{\sigma}}_0, \\ & \boldsymbol{\sigma}(t_f,\mathbf{a}_{N_p})=\boldsymbol{\sigma}_f, \\ & \dot{\boldsymbol{\sigma}}(t_f,\mathbf{a}_{N_p})=\mathbf{0}, \\ & \mathbf{A}_{C2}\mathbf{a_S}=\mathbf{0}, \\ & \mathbf{f}_{rot}(\mathbf{a_S})=\mathbf{0}, \end{array} \tag{34}$$

where $\mathbf{A}_{LS}{\in}\mathbb{R}^{5N_p\times 6N_p}$ and $\mathbf{b}_{LS}{\in}\mathbb{R}^{5N_p}$ stack the LOS matrix $\mathbf{A}_L$ (diagonally) and the vector $\mathbf{b}_L$, see (13), respectively. The parameter $\mathbf{u_S}_{max}{\in}\mathbb{R}^{N_p}$ is a stack vector whose components are all equal to u_{max}. $\mathbf{A}_{rend}{=}[\boldsymbol{\Theta}_{6\times 6(N_p-1)},\ \mathbf{Id}_{6\times 6}]$ is employed to impose the rendezvous condition. The matrix $\mathbf{A}_{C2}{\in}\mathbb{R}^{3(N_p-1)\times 3(m+1)N_p}$ collects all the C^2 continuity constraints developed in (24)-(26). $\mathbf{f}_{rot}{\in}\mathbb{R}^{N_p}$ contains the rotation MRP unit norm constraint, see (29), for each interval. A NLP solver is need to solve the optimization problem (34).

4.3 Initial guess computation

The NLP problem (34) needs an initial guess to start the computation of the optimal solution. The initial guess obtention is composed of two steps: firstly, a six thrusters spacecraft model with three-degrees of freedom is used to formulate and solve a linear programming (LP) problem; then, this LP solution is converted to the NLP decision variables, $\mathbf{u_S}$ and $\mathbf{a_S}$.

Six thrusters problem formulation

Considering a pair of thrusters available on each LVLH direction, the control can be expressed at the end of each sampling interval as $\mathbf{u}_k{=}[u_{x,k},\ u_{y,k},\ u_{z,k}]^T$, hence, the state propagation is linear: $\mathbf{x}_k{=}\mathbf{A}\mathbf{x}_{k-1}{+}\mathbf{B}\mathbf{u}_k$. The LP optimization problem is posed in the same way as in Vazquez et al. (2017) but taking care of bounding the impulses in a conservative way to not overpass the single-thruster maximum impulse amplitude at any time. Moreover, a constraint on the final impulse has to be added to respect the NLP final attitude constraint.

Six thrusters solution transformation to a single-thruster solution

Once the impulses in three directions, $\mathbf{u}_k$, are obtained, the single-thruster impulse amplitude can be computed as $u_k{=}\|\mathbf{u}_k\|_2$. To obtain the attitude parameters, $\mathbf{a}_k$, the MRP at the nodes are obtained and then, a linear system of equations, to fulfill the C^2 continuity conditions at the nodes, is posed as in Caubet and Biggs (2015). A smooth attitude profile is obtained if MRP from nodes without firings ($u_k{=}0$) are interpolated using the MRP of the nodes with impulsive actuation ($u_k{>}0$) as interpolants.

The obtention of the MRP at the nodes is based on the rotation angle and axis. Denoting by m_i the variable that stores the node k at which an impulse ($u_k{>}0$) is given or an attitude has to be reached (instant t_{N_p}), one can obtain the unitary vector $\mathbf{v}_{m_i}$ representing the direction of the impulse as $\mathbf{v}_{m_i}{=}\mathbf{u}_{m_i}/\|\mathbf{u}_{m_i}\|_2$. Using the impulses directions, $\mathbf{v}_{m_i}$, it is possible to obtain the $\boldsymbol{\sigma}_{rot}$, that represent the rotation between these orientations. Therefore, the rotation MRP between t_{k-1} and t_k is

$$\begin{array}{l} \boldsymbol{\sigma}_{rot_{k/k-1}}=\mathbf{e}_{m_i}\tan(s_k\theta_{m_i}/4),\ \ s_k=\dfrac{k-m_{i-1}}{m_i-m_{i-1}}, \\ t_k,t_{k-1}\in[t_{m_{i-1}},\ t_{m_i}]. \end{array} \tag{35}$$

The rotation angle and axis of (35) are obtained from the unitary vectors computed with the aid of the impulse orientation

$$\theta_{m_i}=\operatorname{acos}(\mathbf{v}_{m_i}\cdot\mathbf{v}_{m_{i-1}}), \tag{36}$$

$$\mathbf{e}_{m_i}=\frac{\mathbf{v}_{m_i}\times\mathbf{v}_{m_{i-1}}}{\|\mathbf{v}_{m_i}\times\mathbf{v}_{m_{i-1}}\|_2}. \tag{37}$$

Since $\theta_{m_i}{\in}[-\pi,\ \pi]$, no singularities arise when computing the rotation MRP. Once $\boldsymbol{\sigma}_{rot}$ is obtained, it is possible to compute the attitude at each node k. MRP at the nodes are determined applying the attitude composition rule (7).

The spline coefficients are computed by imposing the attitude at the nodes and C^2 continuity conditions between adjacent intervals. There will be $12N_p - 6$ equations and $3(m+1)N_p$ degrees of freedom. To close the system, it is necessary to add $3N_p(m-3)+6$ equations and $m \geq 3$. Initial and final angular velocities are imposed which adds 6 equations, the remaining $3N_p(m-3)$ equations could be obtained by imposing up to C^{m-1} continuity conditions between adjacent intervals. The previous considerations constitute a linear system of equations trivial to solve.

5. SIMULATION RESULTS

5.1 Rendezvous model

It is important to remark that although a translational linear model has been used for the optimal control computation, the simulations showed in this section has been obtained with the non-linear translational dynamics model as in Gavilan et al. (2012).

Regarding model parameters, the target vehicle flies in a circular orbit at 600 km of altitude, which means that R=6978 km and n=1.0831·10^{-3} rad/s. Chaser vehicle inertia matrix on its principal axis is chosen to be the one corresponding to the CNES lightweight satellite MYRIADE, see Louembet et al. (2009),

$$\mathbf{I} = \begin{bmatrix} 28 & 0 & 0 \\ 0 & 45 & 0 \\ 0 & 0 & 40 \end{bmatrix} \text{kg} \cdot \text{m}^2. \tag{38}$$

The LOS area for all simulations is defined with the parameters: y_0=z_0=2.5 m and c_y=c_z=1/ tan(π/4). Total manoeuvre time is t_f=900 s with a planning horizon of N_p=20 resulting in sampling intervals of T=45 s. Departure point is chosen as $\mathbf{x}_0$=[400, -250, -200]^T m with initial velocity $\dot{\mathbf{x}}_0$=[1, 1, -1]^T m/s. Maximum available impulse and torque are taken as u_{max}=1 m/s and M_{max}=0.02 N·m respectively. The thruster impulse orientation expressed in the chaser body axes is taken as $\mathbf{v}$=[0, 0, -1]^T. Initial angular velocity value is $\boldsymbol{\omega}(0)$=[0, 0, 0]^T s^{-1}. Using a 123 Euler angles sequence, the initial attitude is $\theta_1(0)$=$\theta_2(0)$=$\theta_3(0)$=0, and the final orientation is chosen as $\theta_1(t_f)$=0, $\theta_2(t_f)$=π/2 and $\theta_3(t_f)$≡free. With this attitude the thruster nozzle points towards the positive x LVLH axis at the end of the manoeuvre.

5.2 Simulation results

Attitude flatness splines are chosen to be cubic which is equivalent to take m=3 in (23). The torque constraint grid is chosen to be of n_M=12 points for each interval. The numerical simulation has been done in MATLAB with *Gurobi* optimization package as LP solver for the initial guess computation whereas IPOPT optimization package is employed to obtain a solution of the NLP problem.

As shown in Fig.1, rendezvous is achieved while LOS constraint is not violated. Initial guess cost (measured in terms of single-thruster) was of 4.120 m/s whereas final cost is of 3.846 m/s implying a 6% reduction on fuel consumption. Achieved final distance to target is 0.1609 m with a relative velocity of 0.1981 mm/s which is a good enough accuracy to start docking operations, see

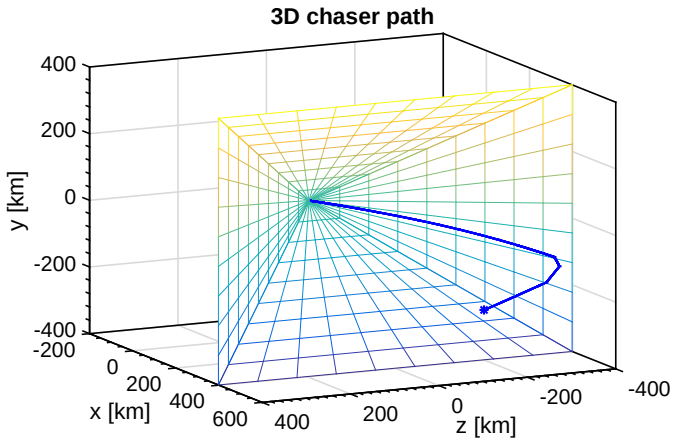

Fig. 1. Chaser 3D path on the LVLH frame.

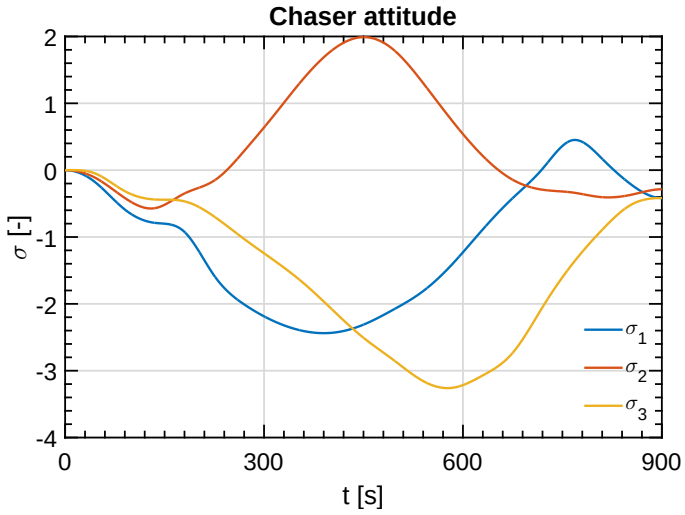

Fig. 2. Chaser attitude.

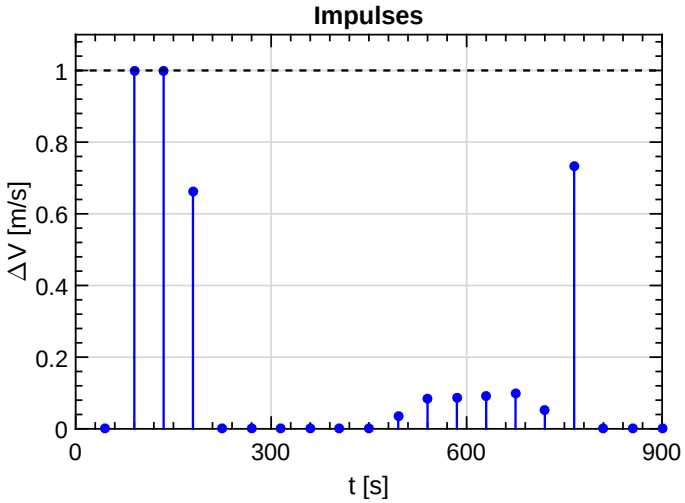

Fig. 3. Computed impulses.

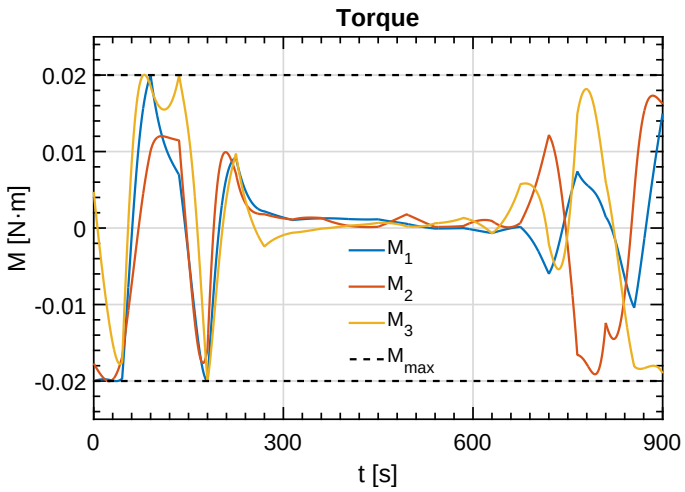

Fig. 4. Computed torque.

Fehse (2003). These deviations are caused by the non-linear rendezvous model used in the simulation. Propulsive effort is concentrated at the start of the trajectory to avoid LOS violation with mid-course corrections to maintain the vehicle inside the allowed area and a braking final impulse to achieve rendezvous. It is worth noticing that this braking impulse is advanced three intervals (the nominal situation is that it takes place at the final time) because the final attitude is imposed.

The considered ACS is able to generate a suitable attitude profile while respecting the problem constraints, see Fig.2 and Fig.4. The attitude profile avoids large rotations by enabling MRP to take norms higher than unity which is equivalent to have a rotation MRP with norm lower than unity at each interval k. The angular velocity profile reveals that major rotations occurs at the beginning and end of the manoeuvre with the purpose of pointing the thruster properly for its first impulse and to reach the final attitude with null velocity respectively. The initial guess torque peak has been lowered one order of magnitude, from 0.2578 N·m to 0.02 N·m.

6. CONCLUDING REMARKS

This paper has presented an algorithm that computes optimal impulse and torque inputs for single-thruster rendezvous scenarios. The algorithm is based on the translational state transition matrix and the flatness attitude property which allows an exact description of the system. Then, the problem is discretized and converted to a NLP problem. A MPC scheme based on linearization around this computed NLP solution could be used to handle with unmodelled dynamics and disturbances. Additionally, the presented formulation could be extended to a chaser spacecraft equipped with an arbitrary number of thrusters.

REFERENCES

Bowen, J., Tsuda, A., Abel, J., and Villa, M. (2015). Cubesat proximity operations demonstration (cpod) mission update. In *Cal Poly CubeSat Workshop*. San Luis Obispo, California, United States of America.

Castellani, L.T., Llorente, J.S., Ibarz, J.M.F., Ruiz, M., Mestreau-Garreau, A., Cropp, A., and Santovincenzo, A. (2013). Proba-3 mission. *International Journal of Space Science and Engineering*, 1(4), 349–366.

Caubet, A. and Biggs, J. (2015). A motion planning method for spacecraft attitude maneuvers using single polynomials. In *AAS/AIAA Astrodynamics Specialist Conference*.

Clohessy, W. and Wiltshire, R. (1960). Terminal guidance systems for satellite rendezvous. *Journal of Aerospace Sciences*, 27(9), 653–658.

Fehse, W. (2003). *Automated rendezvous and docking of spacecraft*. Cambridge University Press. Cambridge, UK, 1 edition. Pp. 171-215.

Fliess, M., Lévine, J., Martin, P., and Rouchon, P. (1995). Flatness and defect of non linear systems: Introductory theory and examples. *Journal of Guidance Control and Dynamics*, 61(6), 1327–1361.

Gautschi, W. (2012). *Numerical Analysis*. Birkhäuser, 2 edition.

Gavilan, F., Vazquez, R., and Camacho, E.F. (2012). Chance-constrained model predictive control for spacecraft rendezvous with disturbance estimation. *Control Engineering Practice*, 60, 111–122.

Guiggiani, A., Kolmanovsky, I., Patrinos, P., and Bemporad, A. (2015). Fixed-point constraned model predictive control of spacecraft attitude. In *American Control Conference*. Chicago, Ilinois, United States of America.

Louembet, C., Cazaurang, F., Zolghadri, A., Charbonnel, C., and Pittet, C. (2009). Path planning for satellite slew manoeuvres: a combined flatness and collocation-based approach. *IET Control Theory and Applications*, 3(4), 481–491.

Marandi, S. and Modi, V. (1987). A preferred coordinate system and the associated orientation representation in attitude dynamics. *Acta Astronautica*, 15(11), 833–843.

Moon, G.H., Lee, B.Y., Tahk, M.J., and Shim, D.H. (2016). Quaternion based attitude control and suboptimal rendezvous guidance on satellite proximity operation. In *European Control Conference (ECC)*. Aalborg, Denmark.

Oland, E., Schlanbusch, R., and Kristiansen, R. (2013). Underactuated translational control of a rigid spacecraft. In *Aerospace Conference (IEEE)*. Big Sky, Montana, United States of America.

Øyvind Hegrenæs, Gravdahl, J.T., and Tøndel, P. (2005). Spacecraft attitude control using explicit model predictive control. *Automatica*, 41(12), 2107–2114.

Persson, S., Bodin, P., Gill, E., Harr, J., and Jörgensen, J. (2006). Prisma - an autonomous formation flying mission. In *ESA Small Satellite Systems and Services Symposium*. Sardinia, Italy.

Vazquez, R., Gavilan, F., and Camacho, E.F. (2017). Pulse-width predictive control for ltv systems with application to spacecraft rendezvous. *Control Engineering Practice*, 20, 199–210.

Woffinden, D.C. and Geller, D.K. (2007). Navigating the road to autonomous orbital rendezvous. *Journal of Spacecraft and Rockets*, 44(4), 898–909.

Zhang, F. and Duan, G. (2012). Integrated relative position and attitude control of spacecraft in proximity operation missions. *International Journal of Automation and Computing*, 9(4), 342–351.